Broadly Tunable Thulium Femtosecond Fiber Lasers Sources around 1.9 - 2.5 μm

D. Klimentov, N. Tolstik, V. V. Dvoyrin, R. Richter and I. T. Sorokina

Abstract — **We report two compact diode-pumped SESAM mode-locked femtosecond thulium-doped all-silica-fiber-based laser systems providing broadband and tunable output in the extremely important mid-infrared spectral range. The first system operates in the Raman soliton regime providing femtosecond pulses tunable between 1.98-2.22 μm. The wide and continuous spectral tunability over 240 nm was realized electronically by changing the amplifier pump diode current. The second system generates the high-energy supercontinuum with the superior spectral flatness of better than 1 dB covering the wavelength range of 1.9-2.5 μm, with the total output energy as high as 0.284 μJ. We simulate the amplifier operation in the Raman soliton regime and discuss the role of induced Raman scattering in supercontinuum formation inside the fiber amplifier . We also report the supercontinuum generation in the highly-nonlinear commercial chalcogenide fiber using the Raman soliton MOPA as an excitation source. Reported systems are promising for a number of applications in the mid-IR.**

Index Terms— **Fiber lasers, Infrared lasers, Optical fibers.**

I. Introduction

HIGH-energy spectrally tunable and/or broadband sources of femtosecond pulses in the spectral domain beyond 2 μm [1–5] are very interesting for many practical applications, including eye-safe LIDAR [6], optical coherence tomography [7], two-photon microscopy, trace gas sensing [8], THz generation, micromachining, high resolution spectroscopy, remote sensing [3, 4], and environmental monitoring. At the same time, the development of such sources is a challenging task.

Optical applications, such as sensing and spectroscopy, require a highly stable supercontinuum (SC) sources. Current publications describe systems, where the SC generation occurs either in the external optical components as specialty fibers [9, 11-14] and waveguides [10], or directly from all-fiber master-oscillator – power amplifier (MOPA) system [4]. The supercontinuum generation in fibers has received much attention of researchers since the first works by R. Alfano et al [11]. Supercontinua in chalcogenide and fluoride ZrF4-BaF2-LaF3-AlF3-NaF (ZBLAN) fibers are reaching out to 2.7 μm [12], 3.6 μm [13] and even 4 μm [14] by excitation at 2 μm, and up to 13 μm in chalcogenide fibers [15] with the pump centered at 4.5 μm.

SC generation in specialty fibers and waveguides usually requires rather complicated scheme and has lower reliability. Specialty fibers and waveguides are often fragile, their implementation as external components requires additional coupling procedure, which increases the sensitivity of the laser system to vibrations, adjustments, often leads to additional losses, and finally substantially decreases the system performance. The direct approach is a significantly simpler, more robust [4] and high output powers are easy reachable. The SC generation directly from the Tm-doped fiber amplifier with average power of 25 W was demonstrated in [16]. However, even more important for a number of applications is the spectral flatness of the radiation. Due to a complex dynamics of supercontinuum generation, it usually has a complex spectral shape. However, the generation of SC of a very flat shape is possible. For instance, SC with the flatness of 10 dB in the spectral range of 1.97-2.43 μm and the maximum average power of 101.6 W has been demonstrated in [17] from the all-fiber system. Here, thulium-doped fiber (TDF) amplifier, pumped by the set of erbium-doped fiber (EDFA) and erbium/ytterbium-doped fiber (EYDFA) amplifiers driven by the DFB pulsed diode, produced ~5-ns pulses at the repetition rate of 2 MHz. However, the generation of top spectrally flat femtosecond SC pulses is a challenging task – this is one of the aims of the present work.

Besides the SC generation, the broadband laser emission coverage can be obtained by tunable fiber lasers. There is a number of techniques for producing high-power ultra-short tunable pulses directly from oscillator [18, 19], and generation of Raman solitons is one of the most advantageous and promising at the moment.

The wide spectral tunability can be obtained by the Raman soliton amplification externally or directly in the amplifier [3, 20]. In particular, tunability over 140 nm range was demonstrated after amplification of Raman soliton in external Tm-doped fiber (TDF) [21], 108 fs pulses with energy of 31 nJ and average power of 3.1 W were obtained. The Er-doped fiber laser (EDFL), used in that work as a seed laser, produced 400-fs pulses, which were transformed into Raman solitons in a passive fiber and subsequently amplified. In another work [22] one-stage master-oscillator – power amplifier (MOPA) system based on EDFL-pumped TDFL seed laser was demonstrated to produce 5-nJ pulses of ~100 fs duration generated directly in the amplifier with average power of ~350

This paragraph of the first footnote will contain the date on which you submitted your paper for review. We would like to acknowledge the NFR project FRITEK/191614, EU FET grant GRAPHENICS (618086) and the Nano 2021 Project N219686.

D. Klimentov (dmitry.klimentov@ntnu.no), I. T. Sorokina (sorokina@ntnu.no), R. Richter (Roland.Richter2@gmx.de) and N. Tolstik (nikolai.tolstik@ntnu.no) are with the Department of Physics, Norwegian University of Science and Technology (NTNU), N-7491 Trondheim, Norway; N. Tolstik is also with the Photonics Institute, Vienna University of Technology, A-1040 Vienna; Austria. V.V. Dvoyrin (v.dvoyrin@aston.ac.uk) with the Aston Institute of Photonic Technologies, Aston University, Birmingham B4 7ET, UK.

mW tunable up to 2.2 μm. More recently, the tunability from 2 to 3 μm was demonstrated [23] from the all-fiber system. The generation of 4-nJ, 100-fs optical pulses was obtained in a germanate glass core silica glass cladding fiber with a driving pulse at 2 μm produced by an all-fiber laser system consisting of an Er-fiber source at 1.6 μm, a Raman fiber shifter, and a Tm-fiber amplifier. Another article describes a chirped pulse fiber amplifier at 2.08 μm tunable up to 2.3 μm emitting 383-fs pulses at the repetition rate of 7 MHz with the pulse energy of 10 nJ [24]. Here, the peak power reached 200 kW level. The simple and compact Tm-doped fiber MOPA generating Raman solitons tunable between 2-2.2 μm with average power up to 3W, pulses as short as 130 fs, and energy up to 38 nJ was demonstrated [20], which is the highest reported pulse energy generation directly from the tunable all-fiber system.

In this paper, we demonstrate two broadband thulium femtosecond fiber MOPAs around 1.9 - 2.5 μm. In the first part of the paper we demonstrate a highly stable all-fiber femtosecond semiconductor saturable absorber mirror (SESAM) mode-locked silica TDF one-stage MOPA operating in the Raman soliton regime with the spectral tunability of 240 nm from 1.98 to 2.22 μm. We realized the wide and continuous spectral tunability electronically, by changing the amplifier pump diode current. We obtained 10-nJ pulses with the duration of few hundred femtoseconds and repetition rate up to 83 MHz. We numerically modelled the performance of the amplifier and compared the experimental results with simulations. We also demonstrated further nonlinear broadening of MOPA output pulses in an external step-index chalcogenide fiber obtaining rather broad SC bandwidth of 680 nm (1.85-2.53 μm) at 168 mW output power.

The second part of the paper is devoted to all-fiber femtosecond SESAM mode-locked TDF one-stage MOPA source of SC generation, which does not rely on the external nonlinear fiber of any type. The spectral coverage of such SC is 450 nm with the 15 dB flatness from 1.95 to 2.4 μm and less than 1 dB at the wavelength range of 2.02-2.34 μm at the average output power of 2.1 W, the overall energy of 0.284 μJ and spectral brightness of 4.7 mW/nm. To the best of our knowledge, these parameters are the highest obtained directly from a compact diode pumped femtosecond MOPA fiber laser.In the present study we are focusing on the role of induced Raman scattering in supercontinuum formation inside the fiber amplifier in anomalous dispersion regime, far from the zero-dispersion wavelength. The continuous amplified pulse breakup and Raman self-frequency shift seem to be the predominant effects in the spectral broadening, assisted by the Tm^{3+} ion gain in the longer wavelength region > 2.1 μm.

II. Experimental

A. Tunable Raman soliton Tm-doped fiber MOPA

A mode-locked TDF laser has been built using the all-fiber linear cavity configuration. Fig. 1 shows the schematic of the laser with one-stage amplifier. The cavity is formed by a butt-coupled commercially available SESAM, a fused fiber coupler used for launching pump radiation into the cavity, a 0.5 m piece of a commercial silica-based TDF, and a fiber loop mirror with the output coupling around 25%. TDF has 9/125 μm core and clad diameters, respectively, and core numerical aperture of 0.15. The optical parameters of the SESAM are as following: 8% modulation depth, 5 % non-saturable losses, and 10 ps relaxation time. Fiber couplers are based on the conventional silica fibers (SMF-28 and SM-2000).

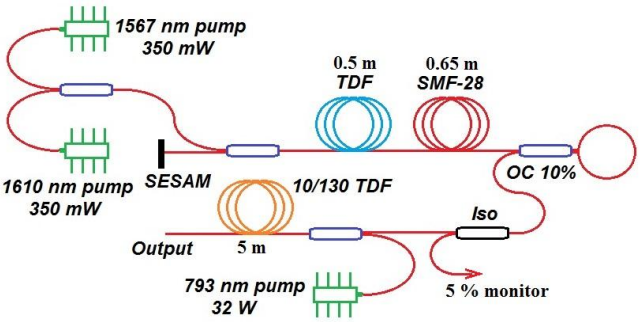

Fig. 1. The schematic of the TDF Raman soliton MOPA system consisting of TDF seed laser and amplifier.

The seed laser was pumped by two 350 mW single-mode laser diodes (Princeton Lightwave Inc.) operating at the wavelengths of 1567 nm and 1610 nm, respectively.

In this laser configuration the cavity had a total length of 1.15 m, resulting in total cavity dispersion of 0.040±0.001 ps/nm [25]. The seed laser output emission formed a stable optical pulse train at the fundamental cavity repetition rate of 83.55 MHz at the wavelength of 1961 nm (Fig. 2a) with the maximum average output power of 5 mW, corresponding to the pulse energy of 60 pJ. No Kelly sidebands were observed. Since the output signal of the seed was below the sensitivity limit of our autocorrelator, we have evaluated the pulse duration from the spectrum as 1.2 ps assuming the transform-limited Gaussian pulses with the spectral FWHM of 4.6 nm. The pulse train was controlled with 60 MHz-bandwidth photodetector and 1 GHz oscilloscope, total response time of the detection system was about 3 ns. The oscillator was operated in the single-pulse regime. At higher pump powers we have also observed harmonic mode-locking regime with double, triple and higher repetition rates. However, this operation mode was unstable and was not used in further experiments.

The one-stage clad-pumped amplifier was based on a 5 m piece of a silica double-clad TDF. The fiber had 10 and 130 μm core and first clad diameters, respectively, and a 0.15 core numerical aperture. The amplifier was clad-pumped at the wavelength of 793 nm by a 32 W CW multi-mode diode laser. The diode laser had an output fiber with a core diameter of 105 μm. The fiber pump/signal combiner was used for coupling of the laser signal and 793 nm pump, and launching of the combined radiation into the active fiber of the amplifier.

The evolution of the MOPA output spectrum at different amplifier pump levels is presented in Fig.2. We logically divided the evolution into three steps: spectral broadening due to the self-phase modulation (Fig. 2b); formation of the first Raman soliton and its spectral shift (Fig. 2c); birth of the

second, the third, and other Raman solitons resulting in the formation of the optical supercontinuum due to their spectral overlap (Fig. 2d).

Fig. 2b presents the behavior of the spectrum at the first step. The amplification exceeded the losses in the amplifier at the pump power of 2.2 W. For the pump power range of 2.93-3.35 W resulting in the average output power of 8.9-20.8 mW, the spectrum experienced weak broadening and mainly symmetrical distortion due to self-phase modulation resulting in appearance of side-lobes.

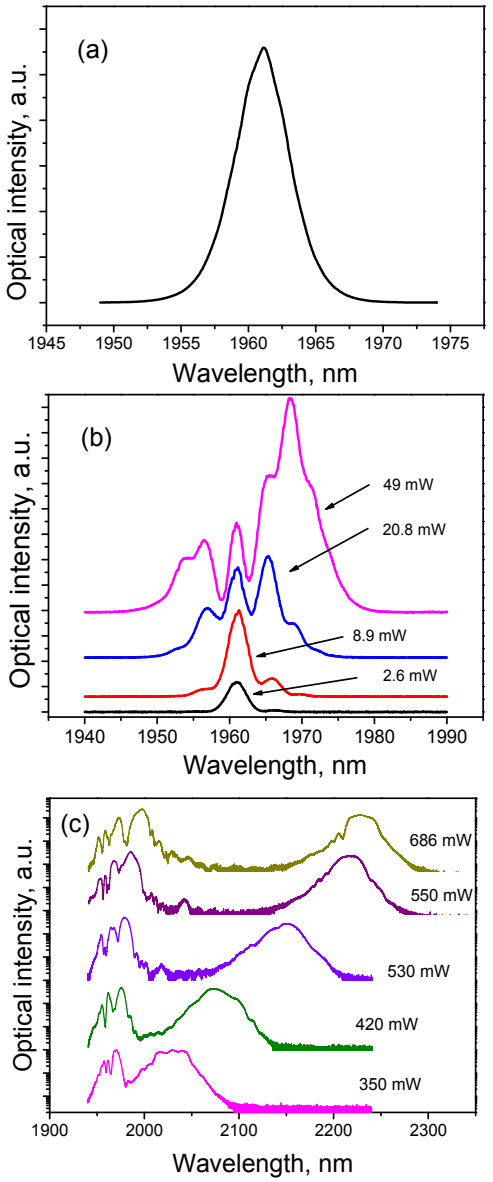

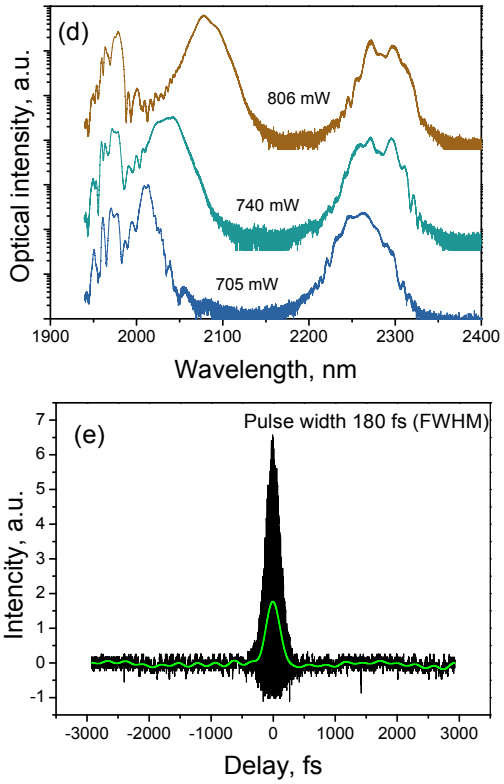

Fig. 2. The seed laser emission spectrum (a); evolution of the spectrum after amplification at low pump powers (b); evolution of the spectrum in the regime of tunable Raman soliton (c), birth and tuning of the second soliton (d); and typical interferometric autocorrelation measured for soliton at 2.09 μm (e) for the high-repetition-rate Raman soliton MOPA.

Starting from 3.35 W of the pump power (20.8 mW of output power), the spectrum became asymmetric. The broadening stopped at the short-wavelength side, while it continued at the long-wavelength side. When the pump power reached 3.6 W resulting in the output power of 49 mW and the pulse energy of 0.6 nJ, the formation of the new spectral component (Raman soliton) began (Fig. 2b). The spectrum became strongly asymmetric. At the pump power of 5.28 W (350-mW output power and 4-nJ pulse energy) Raman soliton shift became distinguishable. With the amplifier pump power changing from 5.28 to 7.8 W (output power increase from 350 to 686 mW), the spectral maximum of the Raman soliton moved from 1.98 to 2.22 μm (Fig. 2c). The spectral width of the soliton band was found to be about 60 - 80 nm FWHM.

Integrating the area under the spectral curve, we have found that the amount of energy in the soliton part in relation to the total output pulse energy slightly varied with the spectral shift from 40 to 62%. The spectral tunability of the first Raman soliton reached 240 nm (Fig. 2c).

The pulse duration notably decreased in the result of the amplification: from 1.2 ps (seed pulse) to 183 fs. The typical interferometric autocorrelation traces for Raman soliton with the spectral position at 2.09 nm (spectrally filtered from residual parental pulse at 1.96 μm) is presented in Fig. 2e. In order to calculate the pulse durations, the autocorrelation traces were Fourier-filtered and fitted by Gaussian function.

Starting from the regime with the output power of 420 mW the pulse duration varied insignificantly.

The further increase of the amplifier's pump power above 7.8 W leads to the further slow red-shift of the first Raman soliton, and also to the birth of new spectral components – the new Raman solitons (Fig. 2d). The strong absorption of silica around 2.4 μm slows down the further red-shift of the first Raman soliton. Further increase of the amplifier pump power should lead to the gradual fill of the gaps between Raman solitons with the subsequent supercontinuum formation. Fig. 4d shows the evolution of the spectrum in the range of the amplifier pump power from 8.2 to 9.1 W (705 – 806 mW of the output power). The slope efficiency of the MOPA is 13% (Fig. 4).

B. Modeling of tunable Raman soliton MOPA

We have modelled the performance of the amplifier. The model consisted of static and dynamic approaches. In frame of the static approach the wavelength- and position-dependent amplifier gain was calculated. The results from the static approach were then implemented into the dynamic model where the short pulse propagation through the amplifying fiber was modelled with nonlinear effects being considered.

In frames of a static approach we used a rate equations analysis. The energy level scheme for Tm^{3+} ions with the levels and transitions involved are shown in the Fig. 3

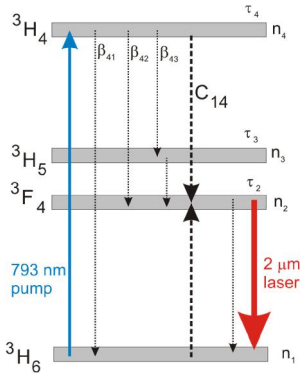

Fig. 3. Energy level scheme of Tm^{3+} levels involved into the modelling.

The set of rate equations is the following:

$$\begin{cases}
\frac{dn_1(z)}{dt} = \beta_{41}\frac{n_4(z)}{\tau_4} + \frac{n_2(z)}{\tau_2} \\
\quad + \frac{P_s(\lambda,z)\xi_s}{A\,h\nu_s}[\sigma_{em}(\lambda)n_1(z) - \sigma_{abs}(\lambda)n_2(z)] \\
\quad - \frac{P_p(z)\xi_p}{A\,h\nu_p}\sigma_p n_1(z) - C_{14}n_1(z)n_4(z); \\
\frac{dn_2(z)}{dt} = C_{14}n_1(z)n_4(z) + \beta_{42}\frac{n_4(z)}{\tau_4} + \frac{n_3(z)}{\tau_3} - \frac{n_2(z)}{\tau_2} \\
\quad - \frac{P_s(\lambda,z)\xi_s}{A\,h\nu_s}[\sigma_{em}(\lambda)n_1(z) - \sigma_{abs}(\lambda)n_2(z)]; \\
\frac{dn_3(z)}{dt} = \beta_{43}\frac{n_4(z)}{\tau_4} - \frac{n_3(z)}{\tau_3}; \\
\frac{dn_4(z)}{dt} = \frac{P_p(z)\xi_p}{A\,h\nu_p}\sigma_{pump}n_1(z) - \frac{n_4(z)}{\tau_4} - C_{14}n_1(z)n_4(z); \\
n_1(z) + n_2(z) + n_3(z) + n_4(z) = n_{Tm};
\end{cases}$$

where n_{Tm} is Tm^{3+} ion dopant concentration; n_1 to n_4 are the populations of energy levels $^3H_6$, $^3F_4$, $^3H_5$, and $^3H_4$, respectively; τ_2 to τ_4 are the lifetimes corresponding energy levels; β_{ij} are branching ratios of the spontaneous transitions from i to j level; C_{14} is the cross-relaxation parameter, P_p is the amplifier pump power at 793 nm; P_s is the signal power at laser transition; A is the area of the Tm-doped fiber core; ξ_p and ξ_s are the overlap factors for the pump and signal mode field with the fiber core; σ_p, σ_{em}, and σ_{abs} are cross-sections for pump absorption, signal emission and signal absorption, respectively.

As a result of a static approach the input-output characteristics of the amplifier were calculated (Fig. 4).

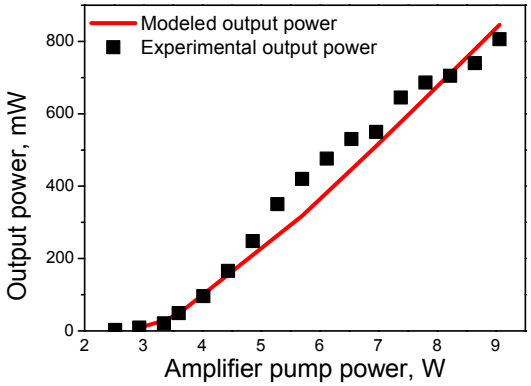

Fig. 4. Input-output characteristics of the Tm amplifier

Then we implemented the split-step-Fourier algorithm to simulate the short pulse propagation in the fiber amplifier. Here the propagation of the full complex amplitude was modelled both in time and frequency domains:

$$A(t) = \int_{-T/2}^{+T/2} A(f)\cdot\exp(-i2\pi ft)df$$

$$A(f) = \int_{-F/2}^{+F/2} A(t)\cdot\exp(-i2\pi ft)dt$$

The pulse coming out of the oscillator was considered as Gaussian pulse. Propagation through both passive bridge fibers and active amplifier fiber was modelled consecutively. Both linear and nonlinear effects affecting the pulse propagation were considered. Wavelength-dependent amplification was calculated using the energy level excitation densities obtained from the static approach (see above). As the silica fiber becomes lossy above 2 μm, the wavelength-dependent loss coefficient provided by the fiber manufacturer was implemented into the model. The group velocity dispersion (GVD) was calculated using the Sellmeier coefficients for fused silica glass [26]. Self-phase modulation and delayed nonlinear response were calculated in time domain according to:

$$\Delta\varphi(t) = \gamma|A(t)|^2;$$

$$\Delta A(t) = i\gamma\left(1 + \frac{i}{\omega_0}\frac{\partial}{\partial t}\right) * \left(A(t)\int_0^T R(\tau)\,|A(t-\tau)|^2 d\tau\right);$$

where

$$R(\tau) = (1 - f_R)\delta(\tau) + f_R h(\tau);$$

$\delta(\tau)$ is the Dirac delta function representing an instantaneous response; $h(\tau)$ is the Raman response function implemented according to Hollenbeck approximation [27]; and f_R specifies the relative strength of the delayed nonlinear response.

The Table 1 summarizes the numerical values of the parameters used for the simulation.

TABLE I
NUMERICAL VALUES OF THE PARAMETERS USED FOR THE SIMULATION

Parameter	Value	Reference
τ_2	430 µs	[28]
τ_3	7 ns	[29]
τ_4	20 µs	[30]
β_{41}	0.88	[31]
β_{42}	0.09	[31]
β_{43}	0.03	[31]
C_{14}	$1.7\cdot10^{-22}$ m^3s^{-1}	[29]
$\sigma_{abs}(\lambda)$	Spectrum	[32]
$\sigma_{em}(\lambda)$	Spectrum	[32]
n_2	3.15	[33]
f_R	0.3	[34, 35]

The MOPA output spectra resulted from the simulations are summarized in the Fig. 5.

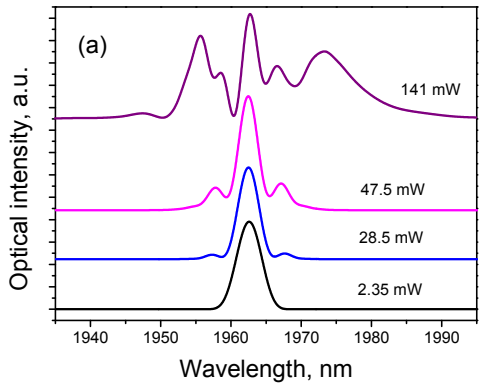

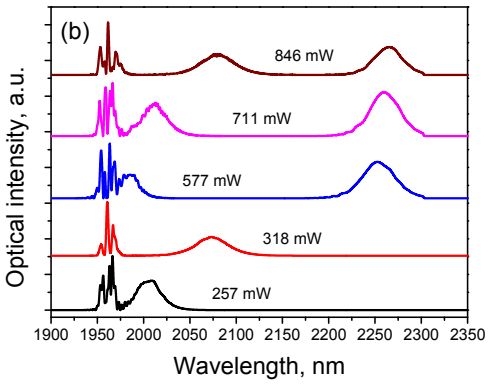

Fig. 5. The simulated evolution of the spectrum after amplification at low pump powers (a); simulated evolution of the spectrum in the regime of tunable Raman solitons (b). The modelled laser output power is shown above each spectra.

The modelled spectra show rather good agreement with the experimental data. Amplification of the seed pulse (Gaussian pulse with 1.2 ps duration) resulted in the spectral broadening induced by SPM (Fig. 5a). Starting from a certain pump power level the formation of first, and then second Raman soliton occurred (Fig. 5b). The good agreement between the modelling and the experiment also confirms the relevance of the seed laser parameters.

C. Analysis of Raman soliton MOPA stability

We have evaluated the stability of the Raman soliton MOPA emission continuously measuring the output power and recording the radio frequency (RF) spectra of the seed laser and the whole MOPA system. The RF spectrum of the seed laser measured with a 200 kHz frequency span and 1 kHz resolution bandwidth is shown in Fig. 6a. The RF spectrum measured with a 2 MHz frequency span and 1 kHz resolution bandwidth is shown in Fig. 6b. A graph at the Fig. 6c illustrates the RF spectrum recorded with 2 GHz frequency span and 1 MHz resolution bandwidth, showing a broad spectrum of harmonics. Rapid drop of the harmonics' intensity is the result of the limited bandwidth of the photodetector (60 MHz cut-off frequency). Experimental results indicate no harmonic mode-locking in the seed laser operation. In order to compare the stability of the seed laser and the amplifier, we measured the same RF spectra at the amplifier output (Fig. 7).

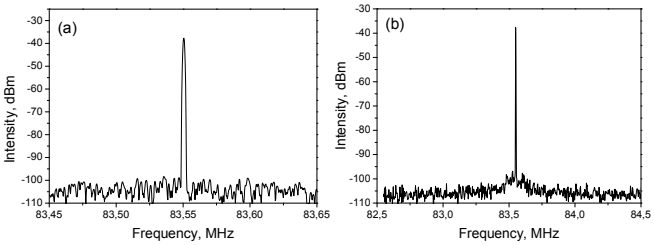

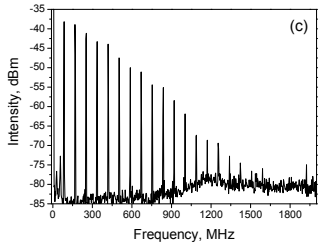

Fig. 6. Measured RF spectra of the seed laser pulses: 200 kHz frequency span and 1 kHz resolution bandwidth (a); 2 MHz frequency span and 1 kHz resolution bandwidth (b); 2 GHz frequency span, 1 MHz resolution bandwidth (c).

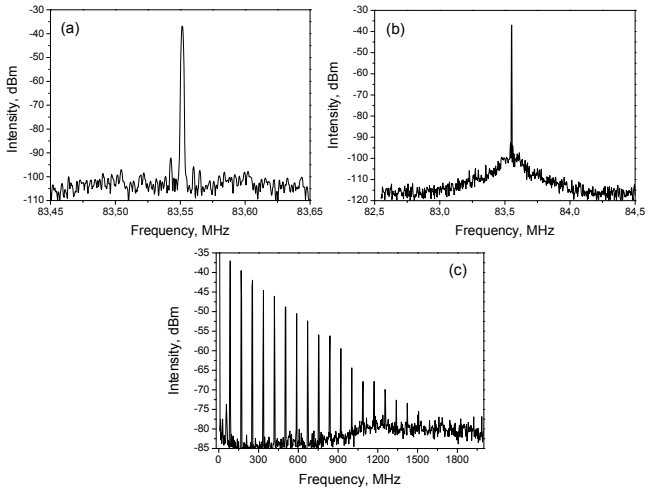

Fig. 7. Measured RF spectra of MOPA output: 200 kHz frequency span and 1 kHz resolution bandwidth (a); 2 MHz frequency span and 1 kHz resolution bandwidth (b); GHz frequency span and 1 MHz resolution bandwidth (c).

The laser system demonstrated stable operation at the fundamental repetition rate. The noise floor for the amplifier was slightly higher, and some artifacts became distinguishable at the level of -95 dB. The power stability was measured during one hour over the frequency range of 0.00027 Hz – 1 Hz. The laser operated at the average output power of 428 mW and standard power deviation reached 2.87 mW, resulting in power fluctuations of less than 1 %.

It is worth noting, that generally the output radiation of the MOPA is not polarized. However, implementation of two polarization controllers (the first one – just after the seed, the second one – just after the amplifier), allowed to obtain controllable near linearly polarized output with polarization extinction ratio of about 1:7.

D. High energy SC generation directly from TDF MOPA

The geometry of the MOPA for direct SC generation (Fig. 8) is similar to the Raman MOPA. It differs by the parameters of the seed laser (cavity length, pulse energy, pump power, emission spectrum), but share the same amplifier.

The seed laser was pumped by a 350 mW single-mode laser diode operating at the wavelength of 1567 nm.

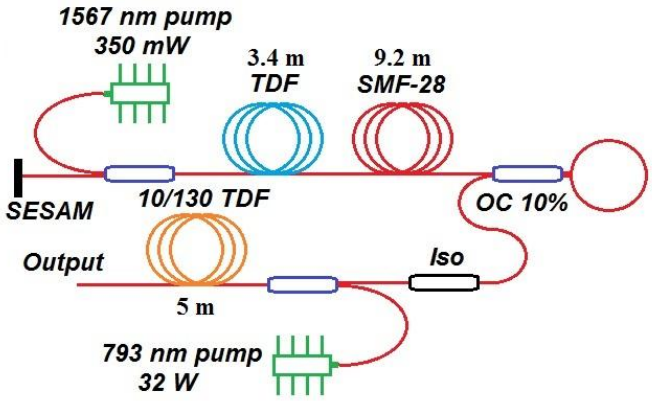

Fig. 8. The schematic of the MOPA system consisting of TDF seed laser and amplifier.

In order to maximize the pulse energy, we have built the cavity with the full length of 12.6 m (3.4 m of TDF and 9.2 m of SMF-28) - the total cavity dispersion of 0.441±0.008 ps/nm. The laser emission wavelength was measured to be around 1985 nm (Fig. 9a). The spectral bandwidth at FWHM was 4.2 nm. The laser operated in the fundamental soliton regime, and Kelly sidebands were observed. The first pair of sidebands was located 3.4 nm apart from the central emission wavelength and carried significant amount of pulse energy. The maximum average output power of the laser oscillator was 10 mW for the single pulse regime where the laser was routinely operated. 20 mW output power could be achieved in the harmonic mode-locking regime. The pulse train measured with 60 MHz-bandwidth photodetector and 1 GHz oscilloscope showed the single-pulse operation at 7.5 MHz repetition rate. The transform-limited pulse duration was about 1.1 ps.

10 mW output power at 7.5 MHz results in >1.3 nJ pulse energy, thus considerably exceeding the maximal soliton energy estimated for 1 ps pulse duration in SMF-28 fiber (0.25 nJ assuming 1 ps pulse duration, 46 ps/nm*km dispersion and $3*10^{-20}$ nonlinearity). We assume that the laser was operated in the pulse burst mode, where the bursts of solitonic pulses separated from each other by 10 to 100 ps were emitted. Our detection system has a response time of about 3 ns and thus could not resolve single pulses in such a burst. Since the laser cavity does not contain any polarization-defining components, vector solitons [36] could be one of the mechanisms responsible for the pulse burst operation.

After amplification of the pulses we achieved the maximum average output power of 2130 mW. The maximum pump power of the amplification cascade reached 14.4 W with the slope efficiency of 17%. Optical gain was detected at 2.2 W of the amplifier pump power. Increasing the amplifier pump power up to ~3.3 W was accompanied by the output power increase without notable broadening of the spectrum. Starting from the amplifier pump power of 3.3 W, the SC formation took place.

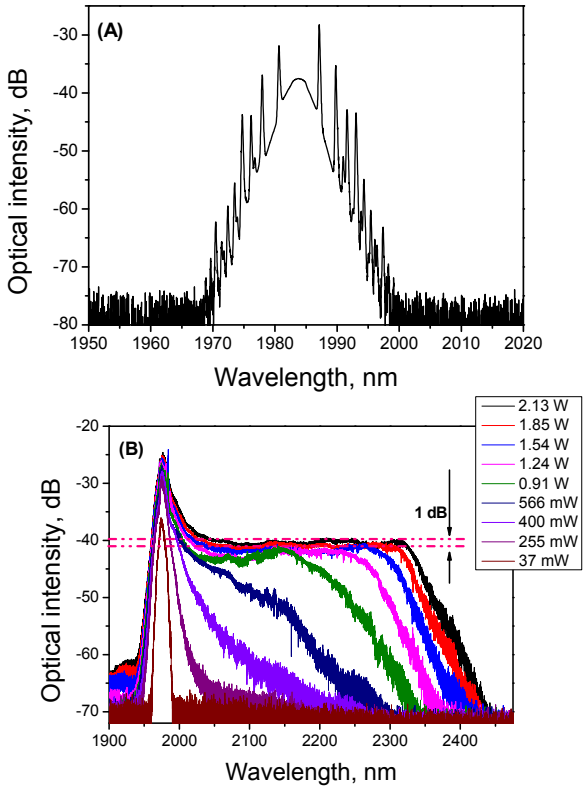

Fig. 9. Seed laser emission spectrum (a), the evolution of the spectra in relation to the output power (b).

Fig. 9b shows the evolution of the spectra in relation to the output power. The spectrum had a flatness of 15 dB at the wavelength range of 1.95-2.4 μm and less than 1 dB at the wavelength range of 2.02-2.34 μm. The spectral brightness reached 4.7 mW/nm.

E. SC in single-mode step-index chalcogenide fiber

In this section we focus on an approach, where supercontinuum generation is produced using an external step-index single-mode chalcogenide fiber. We used the Raman soliton MOPA (Fig. 1) as a pump source. The experimental setup for SC generation in the chalcogenide fiber is schematically shown in Fig. 10.

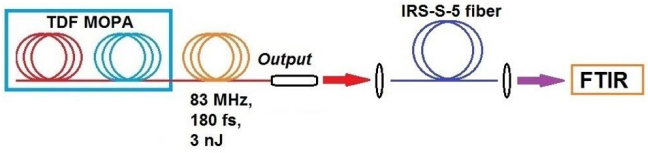

Fig. 10. Schematic of the setup for mid-IR femtosecond supercontinuum generation in nonlinear fibers.

The laser output was focused by a lens and coupled into the nonlinear fiber. The emission from the fiber output was delivered either to spectrometer or to power meter. The launched energy was varied by changing the MOPA energy. The back reflection from input facet of the nonlinear fiber did not affect the stable operation of MOPA, which had a fiber optical isolator at the output.

As a nonlinear fiber, we used a 15 cm piece of the step-index single-mode chalcogenide fiber IRF-S-5 produced by IRflex. The fiber had the core diameter of 5 μm and the cladding diameter of 100 μm, the NA was 0.3. The zero dispersion wavelength was estimated to be 6 μm.

Figures 11(a-e) show the evolution of the spectra before and after propagation through 15-cm nonlinear fiber for different pump energies. The pulse energy of pump varied from 5.6 to 9.7 nJ, resulting in the increase of the energy of the output pulses from 1.1 to 2 nJ. The coupling efficiency into the chalcogenide fiber was 20 - 25%. Fig. 11e shows the broadest spectral coverage of 680 nm, from 1850 to 2530 nm. The output power in (e) reached 168 mW. The spectra had flatness of ~9 dB at the wavelength range of 2.02-2.45 μm.

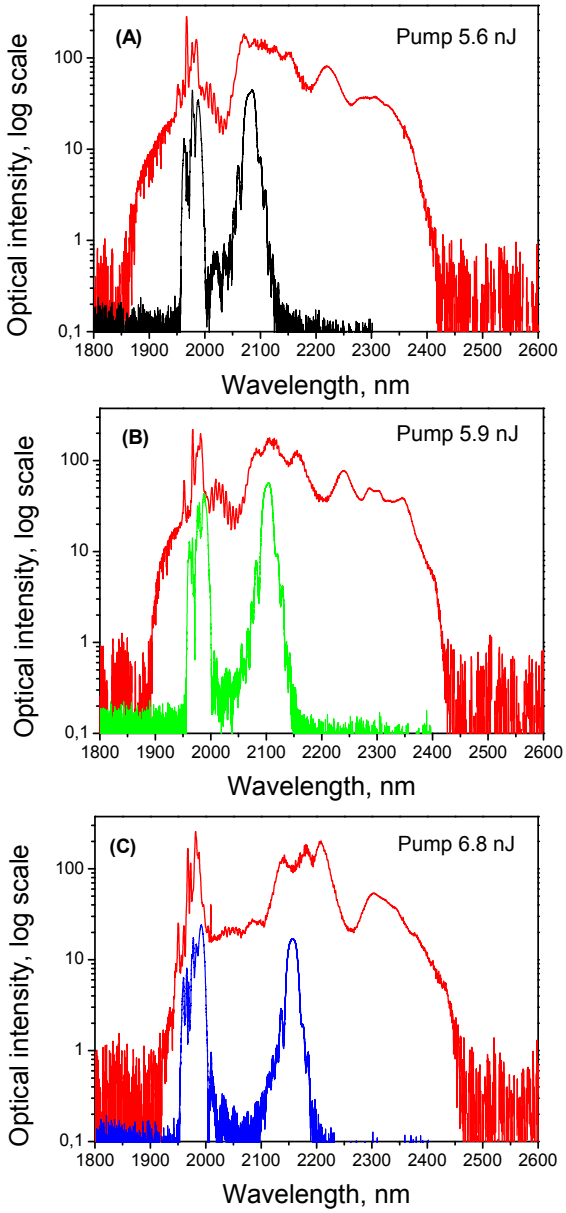

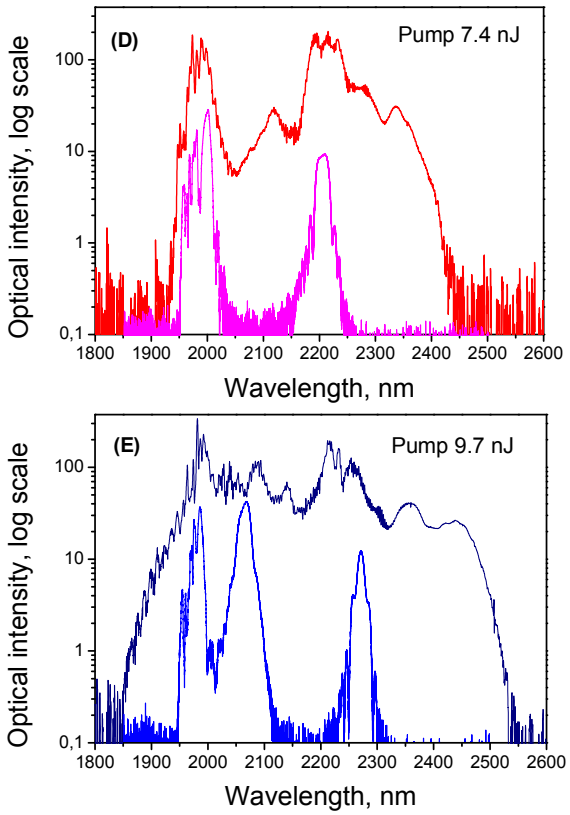

Fig 11. Spectra of femtosecond pulses after propagation in 15 cm step-index single-mode chalcogenide fiber IRF-S-5 at different pump pulse energies.

So far as in our experiment the fiber had a normal dispersion, there was no pulse self-compression and solitons were not supported. The <200-fs pulses from the MOPA output suffered substantial dispersive broadening during the first millimeters of a nonlinear fiber, where the strongest SPM occurred. The elongation of the fiber did not much affect the SC efficiency, and the 15-cm length was chosen as the minimal convenient length to work with.

The experimental results confirm that high nonlinearity of the chalcogenide fiber allows obtaining broader optical supercontinuum at considerably lower pump level, namely, two orders of magnitude lower pulse energy in comparison with the experiment on direct SC generation in TDF MOPA. The use of higher pump power and improved coupling efficiency will allow as obtaining even broader spectrum.

III. DISCUSSION

The process of pulse spectral broadening in Raman amplifier in the anomalous dispersion regime can be understood as follows: when the energy of the picosecond fundamental soliton with soliton number N=1 rapidly increases due to the amplification, the self-phase modulation leads to the gradual spectral broadening of the pulse. At the certain distance much shorter than the dispersion length, the pulse exceeds the maximum soliton energy and eventually breaks up. The sub-soliton will differ from the original picosecond soliton in terms of bandwidth, duration, - and thus energy. Basically it will have the bandwidth corresponding to the SPM-broadened bandwidth of the parental pulse. If its bandwidth is broad enough, the sub-soliton will experience Raman self-frequency shift and time delay [37]. This process occurs at a distance of L_D/N, where N is the soliton number [37], which can occur well within the 4-m long amplifier (L_D~5 m for a 1 ps pulse and β=-100 ps^2/km).

As the Raman-shifted sub-soliton experiences self-frequency shift and moves away from the amplifier gain spectral region, its energy will stop to increase. Moreover, the soliton will begin to gradually loose energy, as the fiber passive losses increase towards the infrared spectral region, thus reducing the self-frequency shift speed. At the same time, the parental pulse will still experience the amplification, and at certain point will break-up again forming the second sub-soliton, which will similarly walk off both in time and frequency. We have seen exactly such behavior both in experiment (Fig. 2) and modelling (Fig. 5)

In the Tm-doped fibers, there is an additional mechanism which could facilitate long-wavelength Raman solitons. In the Tm^{3+} ions, two different transitions may contribute to the amplifier gain:

1) The $^3F_4$-$^3H_6$ transition covering the 1.8–2 μm spectral region and
2) The $^3H_4$-$^3H_5$ transition covering the 2.2–2.5 μm spectral region [38, 39].

At pumping at 793 nm, the gain in the 1.8–2 μm region occurs following the well-known cross-relaxation mechanism in the Tm^{3+} ion [40], which populates the $^3F_4$ level. This process requires high doping concentrations [38, 39]. At Tm^{3+} ion concentrations used in this work the cross-relaxation does not occur with 100% efficiency, so that a certain population is always present at the $^3H_4$ level. This would provide nonzero gain at the $^3H_4$-$^3H_5$ transition, which is four-level and which is not saturated by the 1.9 μm radiation. Thus, the Raman-shifted solitons which are generated in the front section of the amplifier would experience an additional amplification in the rear section of the amplifier at 2.2–2.5 μm wavelength region at no extra cost. The contribution of this mechanism is difficult to estimate at this point, given the scarcity of spectroscopic and manufacturer data for the fiber.

If we would consider now the initial pulse to be not a single pulse, but a burst of pulses, which could generally differ from each other in energy and duration, then each of the pulses in a burst would experience the nonlinear effects described above. Still the energy required for the pulse to break-up will remain more or less constant for all pulses in a burst. As a result, every pulse in a burst will break up at its particular distance while keeping comparable energy. Every of Raman soliton will then have different propagation distance and different Raman shift. The superposition of these pulses will lead to the formation of a top-flat supercontinuum.

Moreover, if the considerable amount of a pulse energy is located in the Kelly sidebands, then the sideband itself can be considered as a sub-ns pulse with a very high soliton number [41, 42]. If such a pulse is being amplified, it could lead to the modulational instability effect [43] contributing to the supercontinuum formation. We have to note here that the generation of SC through both multiple soliton generation and

modulational instability is associated with pulse to pulse fluctuations at the output of the amplifier even if the input from the seed laser is stable. This should lead to decreased level of coherency of the output spectrum – the assumption, which still needs to be verified, and is the subject of a separate study.A separate study is also required to evaluate and compare the individual contributions of the discussed above physical mechanisms to the supercontinuum generation inside the amplifier.

Alternatively, the system configuration described in the Chapter 2E produces the supercontinuum in the normal dispersion fiber. Here the spectral broadening process is driven by the SPM effect only, and the soliton formation does not take place. Such a mechanism usually results in formation of a highly coherent supercontinuum, subject to the seed pulse is short enough. At the same time the spectral flatness of such a supercontinuum is typically rather low. The difference with the SC produced in the chalcogenide fiber in the normal dispersion region is distinctly observable (Fig. 12).

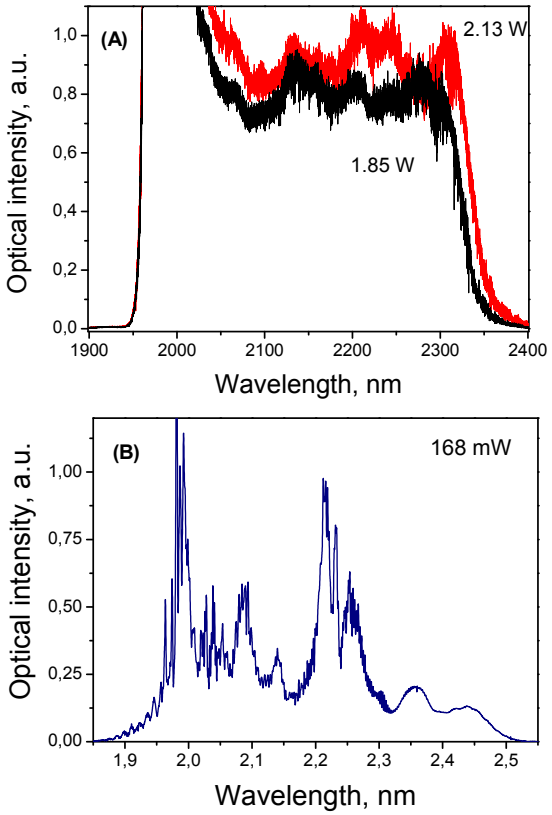

Fig. 12. Spectra of SC generated directly from MOPA (a) and from chalcogenide fiber (b) shown in linear scale.

In spite of the fact that output powers of tens of watts from similar systems have been already demonstrated, many applications require significantly lower output powers. High peak and average power required for generation of SC in silica-glass fibers can be an issue for a number of applications and subsequent attenuation is an inefficient and potentially dangerous solution. Therefore, a low-repetition rate seed laser, coupled to highly nonlinear fiber is a cost-effective and promising way. We used chalcogenide fiber and achieved SC generation in the slightly wider band but at sufficiently low optical powers. Thus, it was <200 mW as compared to 2 W of output power for the SC generated in the silica-based fiber.

IV. Conclusion

We reported two the SESAM mode-locked, femtosecond, thulium-doped-silica-based fiber MOPAs, operating in the Raman soliton regime and high-power supercontinuum generation regime, respectively.

In case of the Raman soliton MOPA, laser generated 5-nJ spectrally tunable <200-fs pulses (1.98 - 2.22 μm) at the repetition-rate of 83 MHz with total average output power up to 0.8 W. While analyzing the system, we have accessed the stability and performed the theoretical modeling of the pulse evolution in the amplifier. The later show the good conformity of theoretical and experimental results.

In case of SC MOPA this allowed obtaining as broad as 450 nm spectral coverage with 2130 mW maximum average output power. At 7.5 MHz repetition rate, this corresponds to the output energy of 284 nJ per pulse. The generated spectrum has a flatness of less than 1 dB and 4.7 mW/nm (0.6 nJ/nm) spectral brightness. These are the highest energy and energy brightness flat-top femtosecond supercontinuum reported in this highly attractive for applications spectral range obtained directly from the silica-based MOPA.

Another approach of the supercontinuum generation has been realized by excitation of a single-mode step-index chalcogenide fiber by spectrally tunable Raman soliton TDF MOPA. In this experiment, we obtained the spectral coverage of 680 nm (from 1850 to 2530 nm) at input average power as low as 200 mW. This approach of SC generation allows obtaining even broader spectral coverage than the first one. The use of commercially available simple step-index chalcogenide fiber makes the setup cost-effective. The relatively large core of the fiber makes all coupling procedures easy.

Sources show a large potential for the development of simple, compact, low cost, and practical high-energy ultra-short pulse lasers systems for optical applications as, for example, sensing and spectroscopy. The Raman soliton lasers are promising for the use in the experiments, where smoothly tunable pulses with relatively high energies are necessary, for example, material processing and as a pump sources for OPO.

References

[1] J. Wu, et al., "Highly efficient high-power thulium-doped germinate glass fiber laser," *Opt. Lett.* vol. 32, pp. 638-640, March, 2007.

[2] S. D. Jackson, et al., *IEEE J. of Selected Topics in Quantum Electronics*, vol. 13, pp. 567-572, May/Jun., 2007.

[3] I.T. Sorokina, et al., "Mid-IR Ultrashort Pulsed Fiber-Based Lasers", *IEEE J. of Selected Topics in Quantum Electronics,* vol. 20, 0903412, Sept/Oct., 2014.

[4] V. V. Dvoyrin, et al., "6.8 W all-fiber supercontinuum source at 1.9–2.5 μm," *Laser Phys. Lett.* vol. 11, 085108 (5pp), June, 2014.

[5] P. Wan, L. Yang, and J. Liu, "High pulse energy 2 μm femtosecond fiber laser," *Opt. Exp.,* vol. 21, pp. 1798-1803, Jan., 2013.

[6] Y. Chen, et al., "Two-channel hyperspectral LiDAR with a supercontinuum laser source" *Sensors,* vol. 10, pp. 7057–66, Jul., 2010.

[7] C. Courvoisier, et al., *Laser Phys.,* vol. 14, pp. 507–514, 2004.

[8] E. Sorokin, Springer NATO Science Series II: Mathematics, Physics and Chemistry (Berlin: Springer), pp. 557–74, 2008.

[9] S. Kedenburg, et al., *Optics Letters*, vol. 40, pp. 2668-2671, June. 2015.

[10] F. Leo, et al., *Opt. Exp*., vol. 22, pp. 28997-29007, Nov. 2014.

[11] The Supercontinuum Laser Source, Robert R. Alfano, ed. (Springer-Verlag), 1989.

[12] Tonglei Cheng et al., "Fabrication of a Chalcogenide-Tellurite Hybrid Microstructured Optical Fiber for Flattened and Broadband Supercontinuum Generation," *JLT*, vol. 33, pp. 333-338, Jan. 2015.

[13] Weiqiang Yang, et al., "High power all fiber mid-IR supercontinuum generation in a ZBLAN fiber pumped by a 2 μm MOPA system", *Opt. Exp.*, vol. 21, pp. 19732-19742, Aug. 2013.

[14] Weiqiang Yang, Bin Zhang, Guanghui Xue, Ke Yin, and Jing Hou, "Thirteen watt all-fiber mid-infrared supercontinuum generation in a single mode ZBLAN fiber pumped by a 2 μm MOPA system", *Opt. Lett.*, vol. 39, pp. 1849-1852, April. 2014.

[15] Petersen, C. R. et al. "Mid-infrared supercontinuum covering the 1.4–13.3 μm molecular fingerprint region using ultra-high NA chalcogenide step-index fibre," *Nature Photon.* Vol. 8, pp. 830–834, Sept. 2014.

[16] V.V. Alexander et al., *Opt. Lett.*, vol. 38, pp. 2292, July. 2013.

[17] Ke Yin, et al., "Over 100 W ultra-flat broadband short-wave infrared supercontinuum generation in a thulium-doped fiber amplifier," *Optics Letters*, vol. 40, pp. 4787-4790 Oct. 2015.

[18] M. A. Chernysheva et al., "Higher-order soliton generation in hybrid mode-locked thulium-doped fiber ring laser," *Selected Topics in Quantum Electronics, IEEE J.,* vol. 20, pp. 425-432, Sept., 2014.

[19] M. A. Chernysheva et al., "SESAM and SWCNT mode-locked all-fiber Thulium-doped lasers based on the nonlinear amplifying loop mirror," *Selected Topics in Quantum Electronics, IEEE J*., vol. 20, pp. 448-455, Sept., 2014.

[20] V. V. Dvoyrin, D. Klimentov, I. T. Sorokina, "3W Raman Soliton Tunable between 2-2.2 μm in Tm-Doped Fiber MOPA," OSA Technical Digest (online) (OSA), paper MTh1C.2, 2013.

[21] P.G. Imeshev, M.E. Fermann, "230-kW peak power femtosecond pulses from a high power tunable source based on amplification in Tm-doped fiber," *Opt. Exp*., vol. 13, pp. 7424-7431, Sept., 2005.

[22] J. Jiang, A. Ruehl, I. Hartl, M. E. Fermann, "Tunable coherent Raman soliton generation with a Tm-fiber system," CLEO, Baltimore, Maryland, USA, CThBB5, 2011.

[23] E. A. Anashkina et al., "Generating femtosecond optical pulses tunable from 2 to 3 μm with a silica-based all-fiber laser system," *Opt. Lett.* vol. 39, pp. 2963-2966, May, 2014.

[24] H. Hoogland, S. Wittek, W. Hänsel, S. Stark, and R. Holzwarth, "Fiber chirped pulse amplifier at 2.08 μm emitting 383-fs pulses at 10 nJ and 7 MHz," *Opt. Lett.*, vol. 39, pp. 735-6738, Dec., 2014.

[25] D. Klimentov, N. Tolstik, V. V. Dvoyrin, V. L. Kalashnikov, I. T. Sorokina, "Broad-band dispersion measurement of ZBLAN, germanate and silica fibers in mid-IR," *JLT*, vol. 30, pp. 1943–1947, June, 2012.

[26] I. H. Malitson, "Interspecimen Comparison of the Refractive Index of Fused Silica," *J. Opt. Soc. Am.,* vol. 55, pp. 1205 Oct., 1965.

[27] Dawn Hollenbeck and Cyrus D. Cantrell, "Multiple-vibrational-mode model for fiber-optic Raman gain spectrum and response function," *J. Opt. Soc. Am. B*., vol. 19, pp. 2886-2892, July, 2002.

[28] P. Peterka, et al., "Thulium-doped silica-based optical fibers for cladding-pumped fiber amplifiers," *Opt. Mater*. vol. 30, pp. 174-176, Sept., 2007.

[29] S. D. Jackson and T. A. King, "Theoretical modeling of Tm-doped silica fiber lasers," *J. Lightwave Technol.*, vol. 17, pp. 948, Jan., 1999.

[30] B. M. Walsh and N. P. Barnes, "Comparison of Tm : ZBLAN and Tm : silica fiber lasers; Spectroscopy and tunable pulsed laser operation around 1.9 μm," *Appl. Phys. B.,* vol. 78, pp. 325, Feb., 2004.

[31] Spector, N., R. Reisfeld and L. Boehm, *Chem. Phys. Lett.* vol. 49, pp. 49-53, July, 1977.

[32] Jackson, S.D., "The spectroscopic and energy transfer characteristics of the rare earth ions used for silicate glass fibre lasers operating in the shortwave infrared," *Laser & Photon. Rev.*, vol. 3, pp. 466-482. Sept., 2009.

[33] T. Kato, Y. Suetsugu, and M. Nishimura, "Estimation of nonlinear refractive index in various silica-based glasses for optical fibers," *Opt. Lett.,* vol., 20, pp. 2279-2281, July, 1995.

[34] A. Ben Salem, R. Cherif, and M. Zghal, "Raman Response of a Highly Nonlinear As2Se3-based Chalcogenide Photonic Crystal Fiber," *PIERS Proceedings*, Marrakesh, MOROCCO, pp. 1256-1260, March, 2011.

[35] Guillermo Salceda-Delgado, Alejandro Martinez-Rios, · Boaz Ilan, David Monzon-Hernandez, "Raman response function and Raman fraction of phosphosilicate fibers," *Opt. Quant. Electron,* May, 2012.

[36] Yu Feng Song, Lei Li,Han Zhang, De Yuan Shen, Ding Yuan Tang, and Kian Ping Loh, "Vector multi-soliton operation and interaction in a graphene mode locked fiber laser," *Opt. Exp*., vol. 21, pp. 10010-10018, Apr., 2013.

[37] J. M. Dudley, et al., "Supercontinuum generation in photonic crystal fiber," *Rev. Mod. Phys*. vol. 78, pp. 1135-1184, Oct., 2006.

[38] J. F. Pinto, G. H. Rosenblatt, and L. Esterowitz, "Tm^{3+}:YLF laser continuously tunable between 2.20and 2.46 μm," *Opt. Lett.* vol. 19, pp. 883-885, June, 1994.

[39] V. Sudesh and J. A. Piper, "Spectroscopy, modeling, and laser operation of thulium-doped crystals at 2.3 μm," *IEEE J. Quantum Electron*., vol. 36, pp. 879-884, July, 2000.

[40] I. T. Sorokina, "Crystalline Mid-Infrared Lasers," in Solid-State Mid-Infrared Laser Sources, I. T. Sorokina and K. Vodopyanov, eds. (Springer Berlin / Heidelberg), pp. 262-358, 2003.

[41] Q. Lin, I. Sorokina, "High-order dispersion effects in solitary mode-locked lasers," *Opt. Commun*, vol. 153, pp. 285-288, August, 1998.

[42] X. Liu, Y. Cui, D. Han, X. Yao, Z. Sun, "Distributed ultrafast fibre laser," *Scientific reports*, vol.5, artile 9101, March, 2015.

[43] A. Demircan, et al., "Supercontinuum generation by the modulation instability," *Opt. Commun*., vol. 244, pp. 181–185, Jan., 2005.